Journal of Hydrology 664 (2026) 134563

Contents lists available at ScienceDirect

Journal of Hydrology

journal homepage: www.elsevier.com/locate/jhydrol

Research papers

Salt migration and export via subsurface irrigation in a saline reclaimed landscape of the Po River lowland (Italy)

Mattia Gaiolini [a], Chiara Sbarbati [a], Abraham Ofori [b], Patrick Habakaramo Macumu [c,d], Maria Pia Gervasio [e], Elena Tamisari [e], Fabio Vincenzi [e], Elisa Soana [e], Giuseppe Castaldelli [e], Vincenzo Piscopo [a], Micòl Mastrocicco [b], Nicolò Colombani [c,*]

[a] DEB – Department of Ecological and Biological Sciences, University of Tuscia, Largo Università snc, 01100 Viterbo, Italy
[b] DiSTABiF – Department of Environmental, Biological and Pharmaceutical Sciences and Technologies, Campania University "Luigi Vanvitelli", Via Vivaldi 43, 81100 Caserta, Italy
[c] SIMAU – Department of Materials, Environmental Sciences and Urban Planning, Marche Polytechnic University, Via Brecce Bianche 12, 60131 Ancona, Italy
[d] GED – Geochemistry and Environment Department, Goma Volcano Observatory, Avenue du Rond Point 142, Quartier Les Volcans, Goma, DR, Congo
[e] DiSAP – Department of Environmental and Prevention Sciences, University of Ferrara, Via Luigi Borsari 46, 44121 Ferrara, Italy

ARTICLE INFO

This manuscript was handled by Dongmei Han, Editor-in-Chief, with the assistance of Ryan T. Bailey, Associate Editor

Keywords:
Upward seepage
Continuous monitoring
Remote sensing
Aquitard
Paleo-channel
Salinization

ABSTRACT

Upward saline groundwater seepage is provoking surface water canals to be salinized in a large, reclaimed area of the Po River lowland in Italy. The salinization is often exacerbated in agricultural fields sub-irrigated via tile drains, which create shortcuts among surface water and shallow groundwater bodies. To identify the causes of salinization and quantify the key sources of dissolved salts, a continuous monitoring of the vadose zone, surface water, and groundwater seepage contributions was established in two adjacent agricultural fields: A1 (≈5 ha) mildly saline cultivated with maize and crossed by a paleochannel and A2 (≈2 ha) saline, left uncultivated and covered by a salt tolerant weeds consociation with the prevalence of Genus *Erigeron* (Asteraceae). The vadose zone continuous monitoring allowed to identify capillary rise as the main driver of soil salinity in A1, while in A2 the capillary rise of groundwater is complicated by additional salt released by root decomposition after mowing, producing a clear EC_{pw} increases up to 20 mS/cm. This information was integrated with remote sensing data on vegetation health (SAVI) and water requirement (NDMI), accounting for the vegetation activity within the field. Piezometers and drainage ditch continuous monitoring allowed for the identification of the surface waters/groundwater relationships and the saline sources in the aquifer/aquitard lenses, revealing a general GW flow toward surface drains as the main source of salinization. EC abruptly increased to 6.5 mS/cm along the SW2 ditch draining A2, while it rose more gradually from 0.55 to 2 mS/cm in the SW1 ditch draining A1. Frequency domain analysis further highlighted internal salinity dynamics, such as increased porewater salinity after mowing in A2, which increased temporary the electrical conductivity up to 20 mS/cm also confirming strong correlations between VWC and EC_{pw} at 60 cm below ground level. Finally, continuous monitoring of water discharge and solute concentrations in the drained ditch enabled the assessment of total salt export during the sub-irrigation period, which was 67.2 ± 6.5 tons (approximately 80 % of the monitoring period). These outcomes show how sub-irrigation can accelerate salinization in shallow groundwater systems under saline conditions.

1. Introduction

Salinization of surface waters (SW) and groundwater (GW) is becoming a common reality in coastal areas and deltaic landscapes around the world (Feist et al., 2023; Loc et al., 2021; Mastrocicco and Colombani, 2021; Seibert et al., 2024). Lowland transitional environments are susceptible to different mechanisms that could trigger water resources salinization, like: (i) atmospheric temperature increase dictated by the ongoing climate change (CC), which in turn increases the evapoconcentration of salts in the topsoil (Thorslund et al., 2021; Van Vliet et al., 2023); (ii) global sea-level rise combined with land subsidence (known as relative sea-level rise) favouring seawater ingression along rivers during droughts and landward GW flow due to increased piezometric heads gradients (Herrera-García et al., 2021; Nicholls et al.,

* Corresponding author.
E-mail address: n.colombani@univpm.it (N. Colombani).

https://doi.org/10.1016/j.jhydrol.2025.134563
Received 14 March 2025; Received in revised form 7 June 2025; Accepted 3 November 2025
Available online 7 November 2025

2021); (iii) overexploitation of water resources for anthropic use that enhances the latter mechanism (Erostate et al., 2020; Petelet-Giraud et al., 2018). Within the Mediterranean area, a renowned hotspot of CC (Lionello and Scarascia, 2018), the Po River delta and its surrounding lowlands is a typical example of such an intricated salinization threat (Gervasio et al., 2023; Straffelini and Tarolli, 2023). Most of the Po River delta and its lowlands rest below mean sea level except for embankments and relic dunes (Da Lio and Tosi, 2019), characterizing this area as a GW discharge zone (Keegan-Treloar et al., 2023). In fact, upward GW seepages have been commonly identified in the most depressed areas typified by high salinity and ammonium (Caschetto et al., 2017; Colombani et al., 2019). These characteristics are typical of many deltaic and lowland areas around the world (De Louw et al., 2013; Jiao et al., 2010; Li et al., 2020).

Despite growing awareness of salinization processes, significant research gaps remain regarding the role of agricultural practices and land reclamation systems in affecting subsurface salinity fluxes. As a matter of fact, the dense network of reclamation canals and the triggered upward seepage has been recognized as an important source of salinization for the inland GW and SW in the Po River lowland (Gaiolini et al., 2024), without deepening into the specific contributions of different stressors nor quantifying their impact on the temporal variability of saline fluxes. This GW saline seepage could make the SW inappropriate for irrigation on a long-term basis due to soil sodification that may impair soil structure and permeability (Tedeschi and Dell'Aquila, 2005). Moreover, the saline return flow could adversely impact the downstream water resources (Beltrán, 1999). In recent years, SW availability has become a concern in the Po River delta and its lowlands, with drier and warmer spells during the growing seasons, when the freshwater demand is at its apex (Bonaldo et al., 2023; Montanari et al., 2023). The ongoing CC is further decreasing freshwater availability in the Po River lowland, due to a decrease in recharge rates coupled with high evapotranspiration rates induced by an increase in atmospheric temperatures (Braca et al., 2019). This has exacerbated the saline GW seepage in the Po River lowland, especially in the most recently reclaimed areas (Gaiolini et al., 2024). A possible countermeasure to limit soil salinization is the sub-irrigation with tile drains, which minimize evaporation (Valipour, 2014) and may help to create freshwater lenses in the shallow aquifer, as recently tested by Zancanaro et al. (2024). However, subsurface drainage systems could increase the salt export towards the downstream channels, and saline fluxes must therefore be monitored and quantified in each relevant environment (Duncan et al., 2008). Thus, to establish the most effective countermeasures to minimize the soil and water salinization in the most depressed inland areas, it's imperative to identify and quantify the salinity sources and to understand the long-term effects of practices such as sub-irrigation and tile drainage on shallow aquifer systems which remain poorly understood.

In response to those challenges and tackle these research gaps, the present study aims to evaluate the GW dynamics of a coastal aquifer within the Po River lowland via time series analysis on integrated field measurements. Recent studies have already depicted peaty lenses as the major source of salinity and postulated a new salinization mechanism due to long-term diffusion from salt stored in plant tissue fragments hosted in peats (Habakaramo Macumu et al., 2024). These findings provided a framework guide for the time-series analysis performed in this study, deepening the understanding of the coastal aquifer and aquitard lenses and their connections with agricultural practices and meteorological drivers.

2. Materials and methods

2.1. Study area

The study site is located approximately 24 km from the Adriatic Sea, near Berra village, within the Po River lowland (Italy). The entire area is characterized by an intensive agricultural activity due to the abundance of freshwater resources and its flat morphology. Fine and organic-rich sediments constituting freshwater swamps and brackish back barrier interbasins are crossed by a network of paleo-channels, in an area mainly lying below the Adriatic Sea level. The complex interplay among lagoonal and littoral environments during the Holocene paleoenvironmental evolution and the reclamation of inland deposits from the 15th to the 19th century (Bruno et al., 2022) made the area particularly heterogeneous with diverse sediment origins, composition, and geochemistry (Amorosi and Sammartino, 2007). These numerous morphological and hydrological changes over the centuries, hydraulic land reclamation, and land subsidence feature these low-lying agricultural lands, posing a hydrogeological risk of flooding and GW salinization that may impact agriculture and the environment (Viero et al., 2019).

The study area (Fig. 1), set in a largely depressed zone from −2 to −3 m above sea level (asl), is experiencing GW and soil salinization mainly due to the presence of seawater and brackish water from the last marine transgression (Amorosi et al., 2008; Habakaramo Macumu et al., 2024). This problem may lead to a reduction of crops production on the midterm in the whole area, represented by the field plot cultivated with maize (A1 in Fig. 1). Conversely, the paleo-seawater trapped in the pore space of low permeability lenses, together with salty halophytes fragments within the peaty horizons, made the A2 plot (Fig. 1) already unsuitable for agricultural production. The latter, which was left uncultivated, was colonized by a salt tolerant weed consociation with the prevalence of Genus *Erigeron* (Bellache et al., 2022). The water table is kept below ground level through an intricate system of reclamation canals and pumping stations. Tile drains were installed in 2018 to drain away excess water and to avoid water-logging conditions. Tile drains are made of steel with an internal diameter of 5 cm, slotted in the upper and lower part. Their depth spans from 0.90 m near the ditches to 0.70 m below ground level (bgl) at the end of the field, with a spacing of 10 m. They were used for sub-irrigation in 2023, leading to a good soybean yield in A1 and the complete loss of the crops in A2. Sub-irrigation was performed by opening the inlet valve from the Albersano irrigation channel and placing removable weirs at the end of SW1 and SW2 ditches.

The climate is temperate, humid subtropical with a monthly average temperature (1940–2024) that ranges from 3.1 °C in January to 25.0 °C in July, with a yearly anomaly of approximately 2.0 °C over the last 5 years (with respect to the baseline period 1951–1980). Yearly average precipitation (1940–2024) is 866 mm, with both positive and negative anomalies during the last decade. Climatic data were retrieved online (on 05/03/2025) from Climate Reanalyzer (https://climatereanalyzer.org/research_tools/monthly_tseries/) cured by the Climate Change Institute, University of Maine.

2.2. Monitoring network

A monitoring network was set up in the field, including piezometers equipped with a Diver® datalogger (Eijkelkamp, Giesbeek, The Netherlands) measuring GW levels (accuracy ±0.5 cm), temperature (T) (accuracy ±0.1 °C), and electrical conductivity (EC) (accuracy ±1 % of reading). The same dataloggers were also placed in the main canals (SW1 and SW2) draining water from the field to monitor SW parameters.

Piezometers were installed approximately 10 m apart from one another in both plots, aligned along the flow line perpendicular to the drainage canals (Fig. 1). Each piezometer was instrumented with multilevel samplers (MLS) for water samples collection and hydrogeological measurements. MLSs consisted of PVC nested mini-wells with an internal diameter of 2 cm, screened in the last 2 cm with a 50 μm Nitex mesh. Each MLS had 5 sampling ports with a 25 cm vertical distance. Different installation depths bgl between the piezometers, intercepting different aquifer layers, allowed the estimation of vertical flow direction, together with EC and T vertical gradient within the GW system, captured in 3 field campaigns: the first done before the sub-irrigation period (27/05/

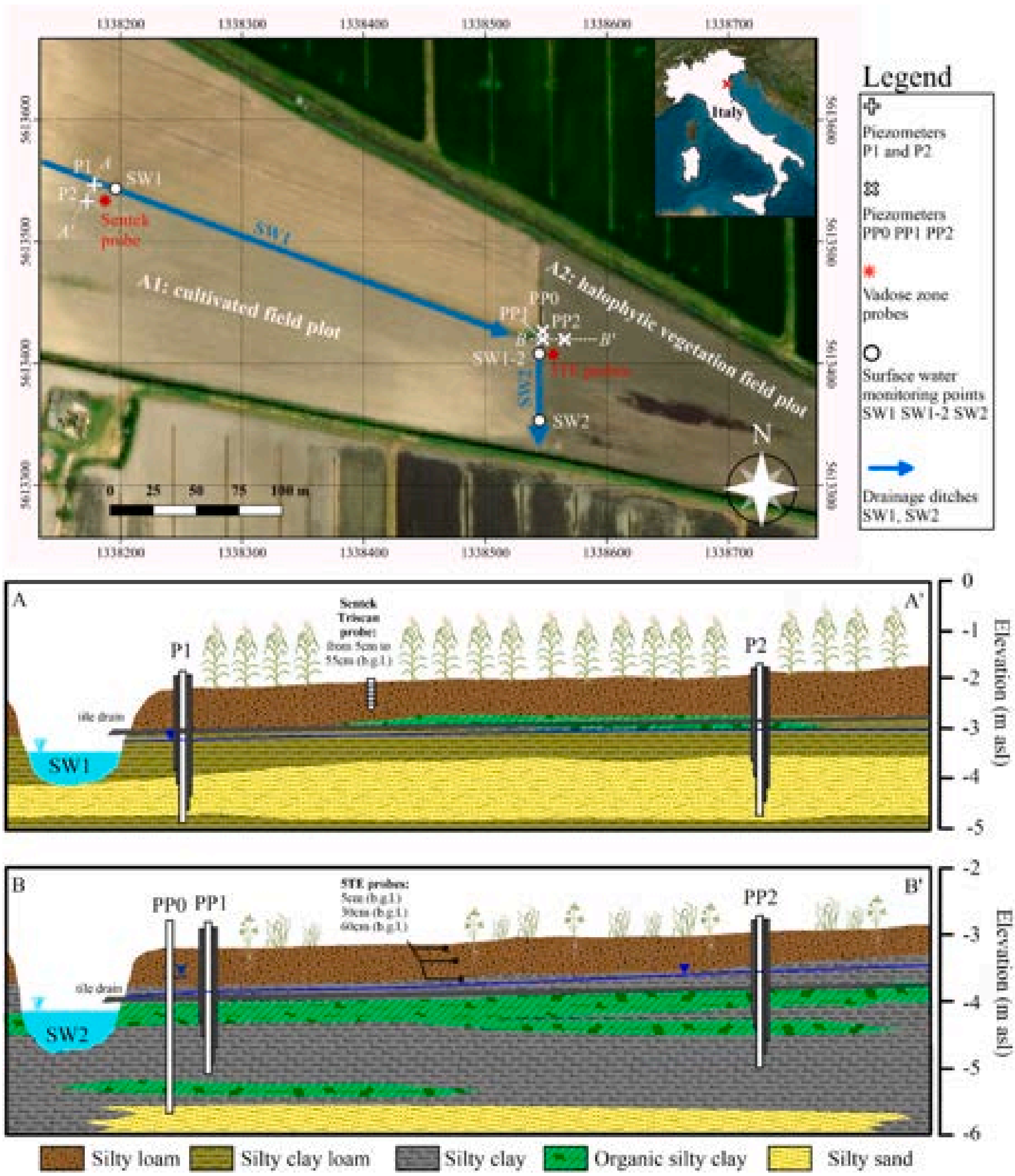

Fig. 1. Map of the study area and monitoring network with the corresponding cross-sections.

2024), the second during the sub-irrigation (09/07/2024), and the third after the harvest (11/09/2024). Dissolved oxygen, pH, oxygen reduction potential, EC, and T were measured with a HANNA Instruments® multiparameter probe (HI98194) along the ditches in a single campaign on the 11th of September 2024. Piezometric heads (m asl) were corrected for atmospheric pressure changes via a Barologger® (Eijkelkamp, Giesbeek, The Netherlands) positioned at the ground surface and referred to the Italian geodetic datum. Furthermore, to delineate the vertical distribution of hydrological parameters and upright flows within the vadose zone, 5TE® Meter probes (Meter Environment, Pullman, WA, USA) were installed in the halophytic plot (A2) at different depths bgl to monitor volumetric water content (VWC), T, and soil bulk electrical conductivity (EC_b) (Fig. 1). EC_b was converted into porewater EC (EC_{pw}) using the Hilhorst (2000) relationship. In the cultivated plot (A1), Sentek–Drill&Drop® probe (Sentek Technologies) were installed to monitor the same parameters at different depths (from 5 to 55 cm bgl). All data-loggers and probes were connected to a Zentra Advanced Cloud Data Logger (ZL6), recording every 30 min for a monitoring period that spans from the 16th of April to the 26th of November 2024, covering more than 6 months. Hourly precipitation data at the closest meteorological station (Avanzarola meteorological station) available on the website (https://simc.arpae.it/dext3r/) of the Regional Agency for Prevention, Environment and Energy of Emilia-Romagna (ARPAE) were downloaded for the monitoring period and cross checked with a manual pluviometer installed at the site and monitored weekly. The R^2 of the weekly cumulated precipitations in both stations was 0.91, and thus the hourly precipitation data of the Avanzarola meteorological station were considered reliable.

2.3. Sentinel-2 data collection

Global Mosaic Service (GMS) Sentinel-2 is an ESA mission aimed at systematically providing high-resolution multispectral imagery of the global terrestrial surface. Data were freely downloaded from the Copernicus Browser (https://Browser.Dataspace.Copernicus.Eu/). Sentinel-2 L2A Soil Adjusted Vegetation Index (SAVI) and Normalized Difference Moisture Index (NDMI) data with a pixel size of 10 m and 20 m, respectively, were collected every 5 days during the monitoring period. Only the data with cloud coverage < 1 % were retained. SAVI is similar to the Normalized Difference Vegetation Index (NDVI) but minimizes soil brightness influences from spectral vegetation indices involving red and near-infrared (NIR) wavelengths (Huete, 1988). The value range of the SAVI is −1 to 1: values from −0.1 to 0.1 correspond to barren areas, values from 0.2 to 0.4 stand for shrub and grassland, and higher values represent green vegetation. NDMI is a moisture index deployed as a proxy of leaf water content that uses NIR and SWIR bands to display moisture (Gao, 1996). This combination can remove the variations caused by leaves' internal structure and leaves' dry matter content, ameliorating the accuracy of vegetation's water content detection. NDMI ranges between −1 and 1: the most negative values correspond to bare soil, negative values between −0.2 and 0.0 represent the wilting point of most plants, positive values between 0.0 and 0.2 are associated with elevated water stress, between 0.2 and 0.4 with low water stress, and higher than 0.4 with optimal conditions.

The integration of these independent and remotely sensed datasets (Fig. 2) was supportive in investigating the role of agricultural practices on the vegetation activity and their impact on the hydrogeological system, that are better discussed in paragraph 3.1.1 of the results.

2.4. Data processing and analytical method

In some cases, sampling procedures along with blocks and failures of the transducers installed in the field end up in erroneous and/or missing data, which results in a little asynchronization of the measurements. This limitation, which could often prevent the use of statistical analysis in the time and frequency domain, was tackled via rigorous data processing. All measured time-series were aligned and synchronized to allow a coherent processing of the datasets, and the records were resampled at a fixed 1-hour using a Doodson filter (Pugh, 1996), ensuring a uniform temporal resolution across the dataset and avoid missing data across the time-series. The Doodson filter (originally developed for tidal data), which operates as a weighted moving average, is particularly suitable for smoothing hydrological datasets, removing the noise without introducing artificial trends. A congruence analysis was then performed to identify potential peaks and errors within the dataset to guarantee that the subsequent hydrological assessments are based on accurate data, enhancing the quality and reliability of the findings. Such an analysis involved a rigorous examination of the data for anomalies and irregularities that could affect the reliability of the research findings.

The processed time-series were then plotted and analysed to evaluate aquifer dynamics and the impact of meteorological drivers and agricultural practices on the system. Recognizing the complex interplay between variables within different compartments of the aquifer and evaluating how they change over time is a complex task that demands sophisticated mathematical and statistical techniques. For a more targeted characterization of the hydrogeological processes that influence the aquifer system (i.e., evapotranspiration, infiltration, capillary rise, irrigation), high and low-frequency components (HF and LF) within each time series were identified, accounting for mechanisms occurring at different time scales. A Low Pass 33 filter tool (LP33) was computed (Emery and Thomson, 2004) on each signal in the MATLAB environment (MathWorks, 2023) to discern phenomena that occur within and beyond 33 h, focusing on distinctive temporal patterns within the dataset (see Supplementary Information). The rationale behind the choice of LP33 was guided by the hydrogeological drivers in the study area (e.g., sub-irrigation events) that operate at periods longer than 24 h. Such a filter is preferred over a 24-hour cutoff filter that might omit important hydrological processes.

Finally, to better assess the associations between variables of

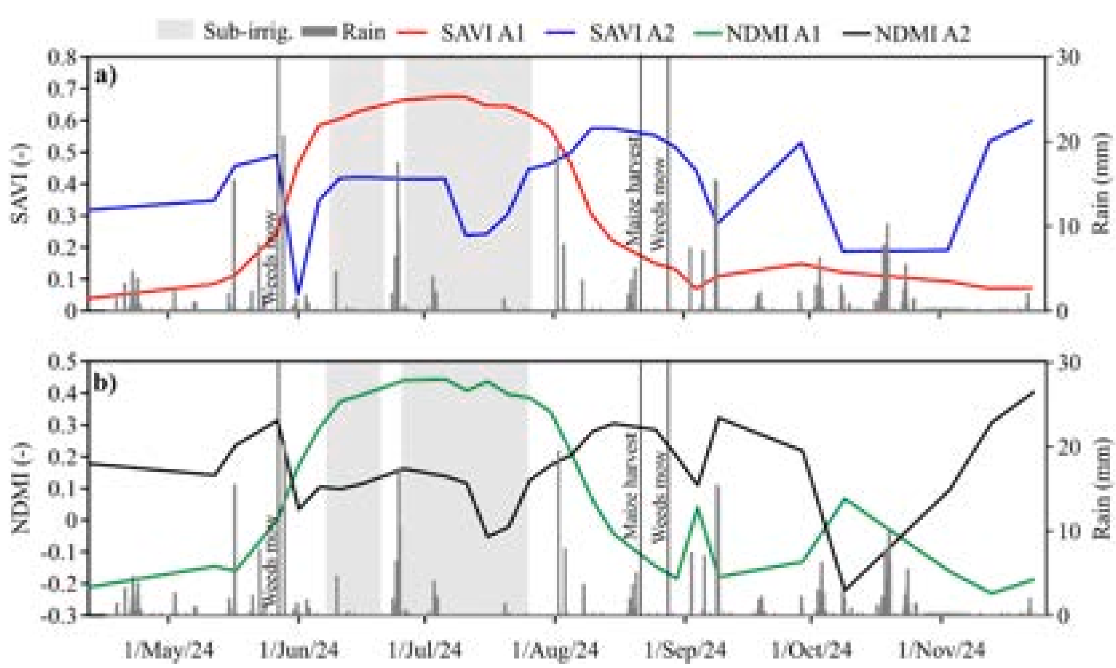

Fig. 2. Time-series plot of (**a**) rainfall (mm), SAVI (–), and (**b**) NDMI (–). Sub-irrigation periods, maize harvest time within the A1 plot, and weeds mowing time within the A2 plot (Fig. 1) are also depicted.

different types over the selected period, a comprehensive statistical approach was pursued by computing Pearson (P), Kendall (K), and Spearman (S) correlation coefficients. The analysis was executed in IBM-SPSS 30.0 (IBM Corp, 2024) environment, evaluating the strength and direction of association between the variables. Correlation coefficient values of ±1 indicate a perfect association, while values closer to zero indicate a weaker relationship. The sign of the coefficient indicates a positive and negative relationship, and among the statistically significant relationships found (p value < 0.05), a minimum effect size of ±0.7 for all the coefficients was set to focus on the larger correlations only.

2.5. Salt export calculation

Data loggers continuously recording water levels and EC of the surface drainage canals (surface monitoring points, see Fig. 1) were instrumental in calculating the cumulative salt export from the agricultural field. A third order polynomial regression curve (see Supplementary Information) was employed as an empirical water discharge rating curve to estimate the outflow rate from the canals; discharge rates were calculated via integration of flow measurements with a portable hand flow-meter or with a bucket and a chronometer during low flow periods (>2.0 l/s). EC-salinity relationship was derived by standard analytical methods (APHA, 2022), and the uncertainty of the estimated salt export was constructed by summing the instrumental accuracies.

3. Results

3.1. Time-series analysis

After being processed and synchronized, all time-series were plotted with the aim of describing the processes occurring: (i) in the vadose zone, (ii) in the saturated zone, and (iii) in the drainage channels. The monitored meteorological conditions, together with agricultural practices performed over the simulation time (i.e., sub-irrigation, maize harvest, and weed mowing), were represented and depicted within the graphs to examine how they affect the GW system.

3.1.1. Time-series analysis of the vadose zone

Fig. 2 focuses on the vadose zone of A1, where VWC, EC_{pw}, and T time-series showed clear variations along the vertical axis. VWC well correlated with rainfall events only at shallower depths (e.g., 5, 15 cm bgl) showing a pronounced increase, as it was directly impacted by precipitation (Fig. 3a). The lower ports recorded values near saturation (approximately 0.45–0.5 m^3/m^3), without reaching it and fluctuating around values of 0.28–0.34 m^3/m^3. Sub-irrigation produced a slight increase in the VWC of the deeper parts of the vadose zone (e.g., 45, 55 cm bgl), related to the rise of the GW table.

During the maize growing season (from June to mid-July 2024, Fig. 2a), where the transpiration is higher (Wang et al., 2021), the VWC decreased only in the topsoil (0–15 cm bgl) due to the continuous water supply from the sub-irrigation and the subsequent capillary rise through the vadose zone, that helped to maintain the VWC near the field capacity. After harvest, the transpiration component ceased, and the plants were removed without any relevant or abrupt impact on the VWC, since the bare soil evaporation component became prevalent.

The EC_{pw} monitored within the vadose zone showed increasing values going deeper, reaching a value of approximately 5 mS/cm in the deepest port, which slowly decreased towards 4 mS/cm in the last month of monitoring (blue line in Fig. 3b). At each rainfall event corresponded an EC_{pw} increase, witnessing a release of salts from the soil, as found by Habakaramo Macumu et al. (2024). The downward solutes transport was limited to the first 25 cm bgl, given that in the lower horizons the VWC increase was limited. EC_{pw} monitored at the shallower depth (5 cm bgl, red line in Fig. 3b) recorded a complex behaviour, showing both decreasing and increasing values during rainfall events, probably due to dilution (EC_{pw} decrease), roots exudates and salts desorption (EC_{pw} increase) from clays and from the soil organic matter (SOM), here abundant and thus behaving as a semipermeable osmotic membrane (Habakaramo Macumu et al., 2024). Moreover, a daily cycle related to the evapoconcentration of salts can be noticed within the first 15 cm bgl (red and orange lines in Fig. 3b) clearly linked with evapotranspiration which is maximal during daytime. No detectable impacts of agricultural practices or precipitation events can be observed in EC_{pw}, except for the continuous rainfall at the beginning of September that

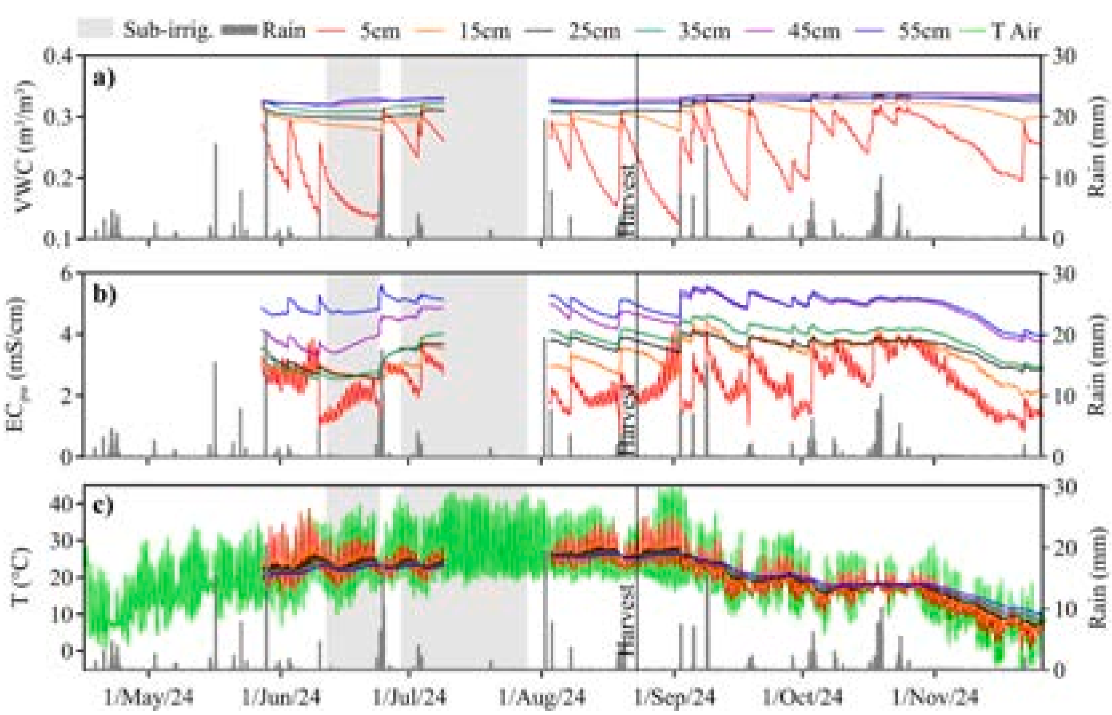

Fig. 3. Time-series plot of (**a**) rainfall (mm), volumetric water contents at different depths (m^3/m^3); (**b**) EC_{pw} (mS/cm) and (**c**) atmospheric and soil temperatures (°C). Sub-irrigation periods and maize harvest time within the A1 plot (Fig. 1) are also depicted.

could have triggered the leaching of roots litter exudates accumulated after the harvest.

The soil temperature followed the seasonal atmospheric temperature trend at all depths within the vadose zone (Fig. 3c), with shallower depths experiencing more pronounced daily fluctuations with respect to the deeper ones due to the thermal dampening capacity of the soil (Evett et al., 2012).

Fig. 3 focuses on the vadose zone of A2, showing VWC, EC_{pw}, and T time-series of only 3 probes, instead of the 6 probes operating in A1, but recording for the whole monitoring period. Again, VWC was well correlated with rainfall events, but in this case at all depths due to a slightly higher soil permeability induced by the extremely high SOM content (Habakaramo Macumu et al., 2024). The lowest port showed VWC values at full saturation just at the beginning of the monitoring period, while the sub-irrigation did not produce any appreciable increase in the VWC throughout the vadose zone (Fig. 4a).

During the growing season of the mildly salt tolerant weeds (from June 2024 to the second weeds mow, Fig. 2), the VWC decreases dramatically at 30 cm bgl, where most of the weeds' roots were located. Here, the VWC almost neared the wilting point without reaching it, since sub-irrigation provided a continuous supply of water transpired by the weeds. Coherently, the probe at 60 cm bgl showed higher VWC values, especially in the second sub-irrigation period, when atmospheric temperatures were elevated and precipitation was almost absent. The EC_{pw} showed lower values at 5 and 30 cm bgl than at 60 cm bgl for most of the monitoring period, with values between 0.1–5 mS/cm for the probe at 5 cm bgl, between 0.3 and 21 mS/cm for the probe at 30 cm bgl, and 4–11 mS/cm for the probe at 60 cm bgl. After the second weeds mowing, the EC_{pw} in the middle port (black line in Fig. 4b) increased up to values of approximately 5 mS/cm due to the heavy rainfall events of September, reaching peaks of 20 mS/cm after the prolonged precipitations of October. Since the mowing did not remove the aerial part of the weeds (that were mulched and left in place), their roots kept releasing salts during the decomposition that leached downward during intense precipitation events. This leaching was limited to the first 50 cm of soil, given that in the lower port the EC_{pw} increase was minimal. The EC_{pw} at 60 cm bgl recorded a notable increase during the sub-irrigation periods that was related to the capillary rise of the GW that had an average EC of 8 mS/cm (see section 3.1.2). The soil temperatures followed the seasonal atmospheric temperature trend, mimicking the A1 results.

The temporal trends of SAVI and NDMI in A1 and A2 followed similar patterns (Fig. 2).

In plot A1, large bell-shaped curves were observed for both the SAVI and NDMI indices, reflecting the increasing vegetation activity and moisture during the maize growing season, supported also by the sub-irrigation phase. While fluctuating patterns are shown by both indices in plot A2 (Fig. 2) due to a consociation of different plant species naturally growing, developing, and competing in these saline soils.

In fact, NDMI was around zero during the sub-irrigation period, indicating stress conditions for the weeds, probably induced by the elevated soil salinity, and/or by other causes like acidic conditions (Habakaramo Macumu et al., 2024). It can be noticed that SAVI decreased to near zero after the first mowing, while it did not after the second one. This was due to the mulched weeds' biomass accumulated on the ground in the second mow that almost completely covered the soil, while in the first mow, the mulched biomass was less abundant and was scattered on the ground.

3.1.2. *Time-series analysis of SW-GW interaction zone*

Fig. 5 focuses on the SW-GW relationships in A1. Precipitation events that spanned throughout the monitoring period were associated with an increase in GW levels in the piezometers P1 and P2, and the drainage ditch SW1 (Fig. 5a).

Water levels in P1, P2, and SW1 responded quickly to rainfall, suggesting a direct connection to shallow subsurface flow and surface runoff. By comparing the monitored water levels (P2 > P1 > SW1), the GW flow was generally directed towards the ditch SW1, which acted as a drain for the surrounding area. Peak rainfall events produced a steeper and higher rise in P1 (brown line in Fig. 5a) due to its proximity to the ditch, resulting in a temporary inversion of the GW head gradient and thus of the flow direction.

The sub-irrigation period corresponded to a rise in both GW and SW1 water levels, with the hydrometric level in SW1 surpassing the position of the tile drain and thus producing a horizontal injection of freshwater into the paleochannel. The capillary rise within the silty sand grain size constituting the paleochannel allowed the GW heads in P1 and P2 to rise

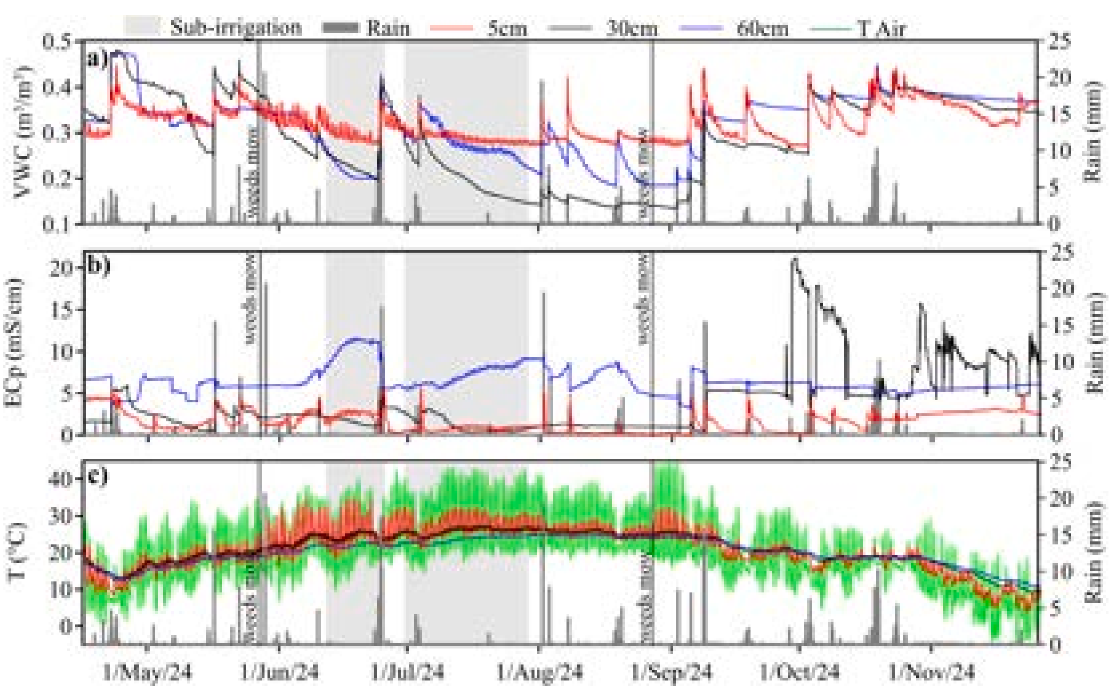

Fig. 4. Time-series plot of (**a**) rainfall (mm), volumetric water contents at different depths (m^3/m^3); (**b**) EC_{pw} (mS/cm) and (**c**) atmospheric and soil temperatures (°C). Sub-irrigation periods and weeds mowing time within the A2 plot (Fig. 1) are also depicted.

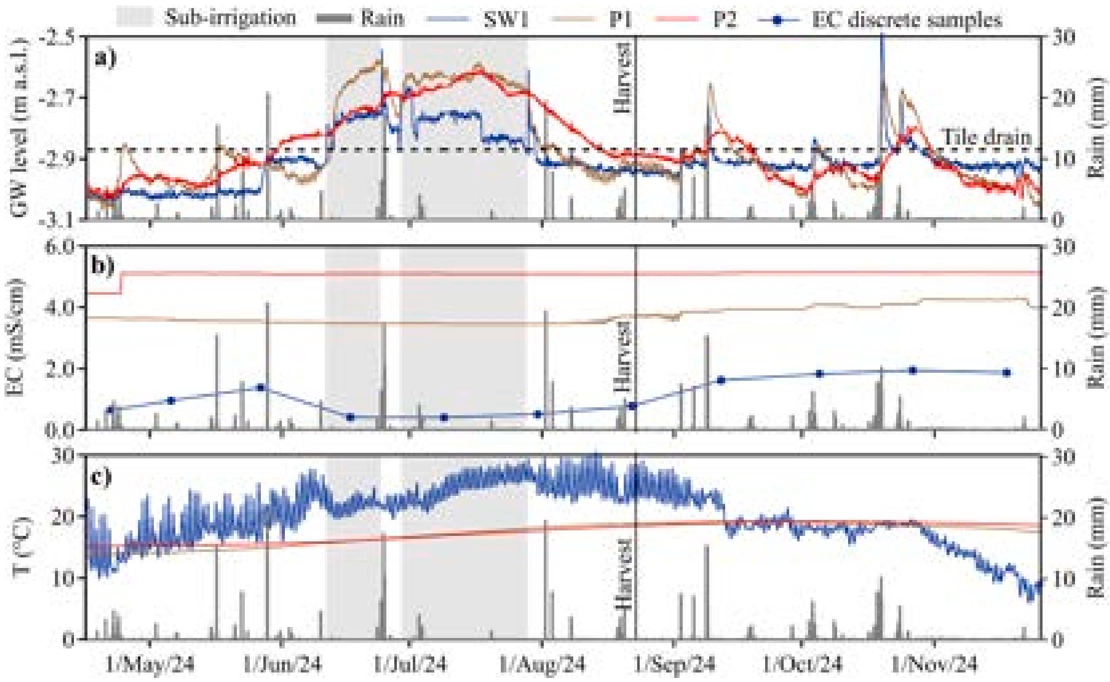

Fig. 5. Time-series plot of (**a**) rainfall (mm), SW1 hydrometric levels and GW levels in P1 and P2 piezometers (m asl); (**b**) SW1 (discrete measurements) and GW EC in P1 and P2 (mS/cm); (**c**) SW1 and GW temperatures in P1 and P2 (°C); sub-irrigation periods, maize harvest time, and the position of the tile drain within the A1 plot (Fig. 1) are also depicted.

more than 0.2 m relative to the SW1 hydrometric level, which is within the expected literature values for these kinds of sediments (Lu and Likos, 2004).

Both piezometers presented a stable EC trend, with values around 5 mS/cm registered in P2 and around 4 mS/cm in P1 (Fig. 5b). Discrete EC measurements in the SW1 drainage ditch during the monitored period (blue dots in Fig. 5b) showed lowest values in coincidence with the sub-irrigation period (below 0.5 mS/cm), that are typical of the Po River water salinity in this area (Marchina et al., 2015). The lower EC values of SW1 indicated GW seepage as the main source of salinity feeding the ditch. This was confirmed by a monitoring campaign along the drainage ditch SW1 and SW2 done on the 11th of September 2024, where the EC passed from 0.41 mS/cm at the SW1 inlet from the Albersano irrigation channel to 6.5 mS/cm at the SW2 outlet (Tab. 1). Also, the other monitored parameters immediately dropped respect to the inlet point, testifying the GW contribution to the SW.

SW1 water temperature mimicked the atmospheric temperature, showing a clear seasonal trend and diurnal oscillations (Fig. 5c). The amplitude of these daily oscillations diminished during the sub-irrigation period due to stable water temperature sourced from the Po River located 2 km North and diverted into the Albersano irrigation channel. The same delayed seasonal trend was observed in both P1 and P2, where no daily fluctuations were detected.

Fig. 6 focuses on the SW and GW relationships in A2. Precipitation events that span throughout the monitoring period were associated with an increase in GW levels in piezometers PP1 and PP2, and in the drainage ditch SW2 (Fig. 6a), like in the previous transect A1. PP0 which monitored the semiconfined aquifer, responded directly to the multiple daily events recorded at the beginning of September, with abrupt increases and decreases, typical of confined conditions.

Table 1
Physical-chemical parameters along the SW1 and SW2 ditches, collected on 11/09/24.

Id	Sample location X (m)	Y (m)	Z (m)	T (°C)	DO (mg/L)	EC (mS/cm)	pH (–)	ORP (mV)	DO_{sat} (%)
IN	264756.6	4,981,731	−1.96	24.11	4.42	0.410	7.63	109.3	50.9
SW1	264881.2	4,981,669	−2.21	24.17	1.31	0.550	6.27	−60.0	15.5
SW1	264904.1	4,981,663	−2.18	22.58	1.35	0.448	6.84	−70.6	15.5
SW1	264931.3	4,981,652	−2.17	24.63	1.29	0.948	6.41	−37.4	15.5
SW1	264959.1	4,981,642	−2.22	23.32	1.32	0.978	6.27	−13.3	15.5
SW1	264,991	4,981,631	−2.22	22.79	1.36	0.906	6.65	−44.8	15.7
SW1	265012.2	4,981,622	−2.26	22.35	1.38	1.171	6.70	−112.0	15.8
SW1	265042.9	4,981,608	−2.29	21.99	1.39	1.946	6.83	−106.5	15.9
SW1	265068.3	4,981,600	−2.31	21.99	1.40	1.945	6.73	−88.2	15.9
SW1	265096.6	4,981,593	−2.37	23.34	1.43	1.838	6.56	−56.4	16.8
SW1	265123.2	4,981,582	−2.38	24.31	1.40	1.920	6.45	−25.1	16.7
SW1	265150.3	4,981,573	−2.62	24.73	1.38	1.919	6.31	6.2	16.6
SW1	265173.9	4,981,562	−2.61	22.02	1.41	1.975	6.21	2.1	16.1
SW1	265199.8	4,981,555	−2.60	22.87	1.46	1.778	6.53	−16.3	17.0
SW1	265,230	4,981,543	−2.63	22.67	1.48	1.798	6.57	−29.8	7.1
SW2	265265.6	4,981,532	−2.68	22.36	1.50	2.012	6.52	−39.0	17.2
SW2	265274.7	4,981,511	−2.95	22.47	1.52	3.631	6.53	−36.7	17.7
SW2	265271.6	4,981,473	−2.98	24.38	1.57	6.430	7.05	−70.4	18.0
OUT	265259.1	4,981,475	−3.12	24.39	1.55	6.501	7.03	−72.3	17.8

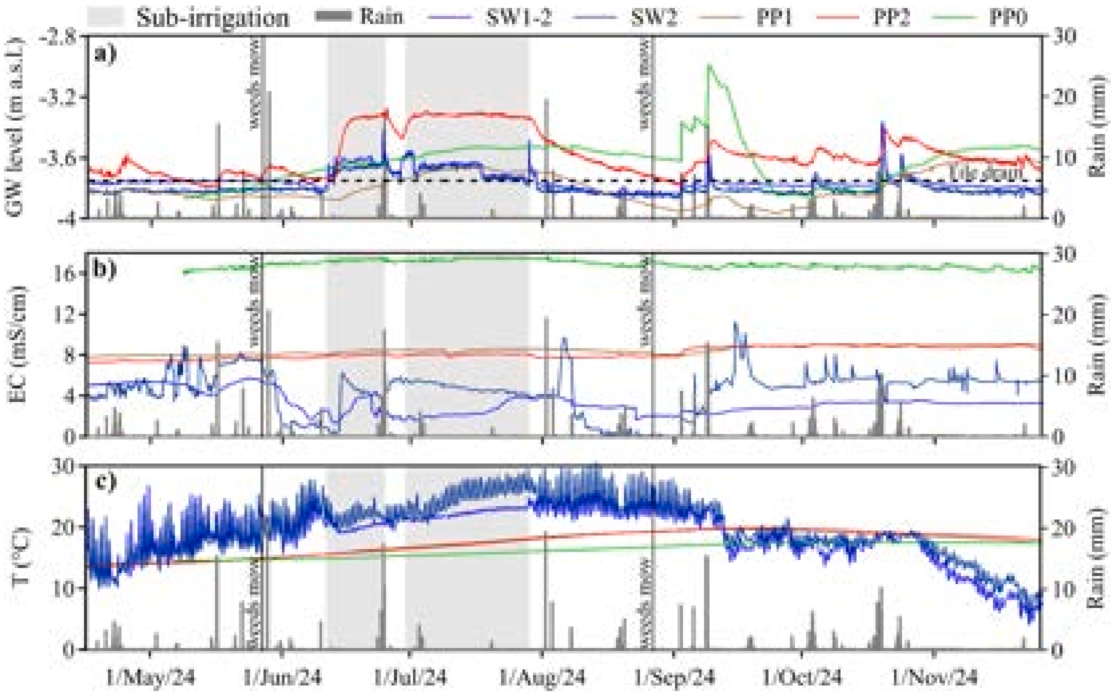

Fig. 6. Time-series plot of (**a**) rainfall (mm), SW1-2, SW2 hydrometric levels, and GW levels in PP0, PP1, and PP2 piezometers (m asl); (**b**) SW1-2, SW2, and GW EC in PP0, PP1, and PP2 (mS/cm); (**c**) SW1-2, SW2, and GW temperatures in PP0, PP1, and PP2 (°C); sub-irrigation periods, weeds mowing time, and the position of the tile drain within A2 plot (Fig. 1) are also depicted.

By comparing the monitored water levels (PP2 > PP0 > PP1 > SW2), the GW flow was generally directed towards the SW2 ditch. Peak rainfall events produced a much smother rise in PP1 than in PP2 due to local changes in sediment texture and thus in hydraulic conductivity (see transects in Fig. 1). PP0 was positioned just a few cm apart from PP1 and thus a continuous upward seepage can be inferred during the monitored period, which through the aquitard lens fed the tile drains and ditches.

The sub-irrigation period corresponded to a rise in both GW, SW1-2, and SW2 water levels, but the piezometric increase in PP1 was much smoother than in PP2. This could be interpreted as a low hydraulic conductivity lens present just in the PP1 location. All piezometers presented a stable trend of measured EC with values around 8 mS/cm in both PP1 and PP2, while PP0, with values around 16 mS/cm, represented the most saline endmember of this shallow GW system and a continuous source of saline upward seepage (Fig. 6b). The continuous SW1-2 EC measurements showed the lowest values in coincidence with the sub-irrigation period (around 2.5 mS/cm), while the SW2 EC recorded twice as high EC, witnessing the large contribution to SW salinization of A2. As previously mentioned, the lack of EC decrease in GW during the sub-irrigation periods is again proof that freshening of shallow GW is hardly being achieved via tile drains. This is not an isolated case but is rather widespread in all the Po River lowland (Colombani et al., 2019; Di Giuseppe et al., 2014).

This is shown in Fig. 7, where the EC depth profiles for all the MLSs used to monitor GW during the 3 field campaigns did not vary significantly at the bottom of each profile. Only in P1, a slight decrease of EC could be noticed in the second sampling port (~1.75 m bgl) during the sub-irrigation period (09/07/24), while in P2 no significant EC variations were detected. On the contrary, the MLSs in plot A2 recorded an increase in EC during the sub-irrigation period (09/07/24) in the upper sampling ports, again witnessing the salt release in GW.

SW1-2 and SW2 water temperatures mimicked the atmospheric ones, showing a clear seasonal trend and diurnal oscillations (Fig. 6c), like in A1. The amplitude of daily temperature oscillations in SW1-2 diminished much more than in SW2 due to riparian vegetation growth. The dampened seasonal temperature trend was observed in PP1 and PP2, like in A1, with PP0 exhibiting the least temperature variability.

3.2. *Frequency domain and correlation analysis*

Frequency domain and statistical analysis was performed considering the entire monitoring period and the sub-irrigation period only to understand the role of these agricultural practices in affecting the salinization dynamics within the study area. The LF and HF components in the entire period did not allow for gaining large significant (<−0.70 or >+0.70) statistical correlation parameters (P, K, and S), except for the soil temperatures that are obviously correlated (see Supplementary Information for the correlation matrix). While LF and HF components were performed only during the sub-irrigation periods, allowed to gain interesting insights. For example, the only significant correlation for the HF component was the negative correlation (−0.82/−0.66/−0.83) among the VWC near the water table (60 cm bgl) in A2 and its EC_{pw}, meaning that sub daily decrease in VWC coincided with an increase in soil salinity, probably due to the plant transpiration.

The LF component statistical analysis in Tab. 2 provided more information on the hydrogeological system depicting the largest significant relationships (<−0.70 or >+0.70, p-values < 0.01) among SW and GW The GW level increase in P2 led to a VWC increase in the lower soil horizons in A1, confirming the role of the sub-irrigation in driving both GW level and VWC. Another positive relationship between PP0 and PP1 (in the A2 plot) confirmed the upward seepage from the most saline portions of the aquifer. The positive correlation of VWC and EC_{pw} in A2 at 30 cm bgl confirmed that this was the horizon most exploited by the saline tolerant weeds spontaneously growing in A2 during the sub-irrigation periods. While the negative correlation found between VWC and EC_{pw} in A2 at 60 cm bgl confirmed that soil salinization was not only occurring due to roots' transpiration (that worked on a sub daily cycle), but mainly due to long term saline upward movement from GW, as the negative effect size of the correlation increases in the LF signal (−0.92/-0.83/-0.96 < -0.82/-0.66/-0.83). Soil and GW temperatures show positive correlation with coefficients that increase considering the deep monitoring ports (e.g., 30 and 60 cm bgl with PP1 temperature in

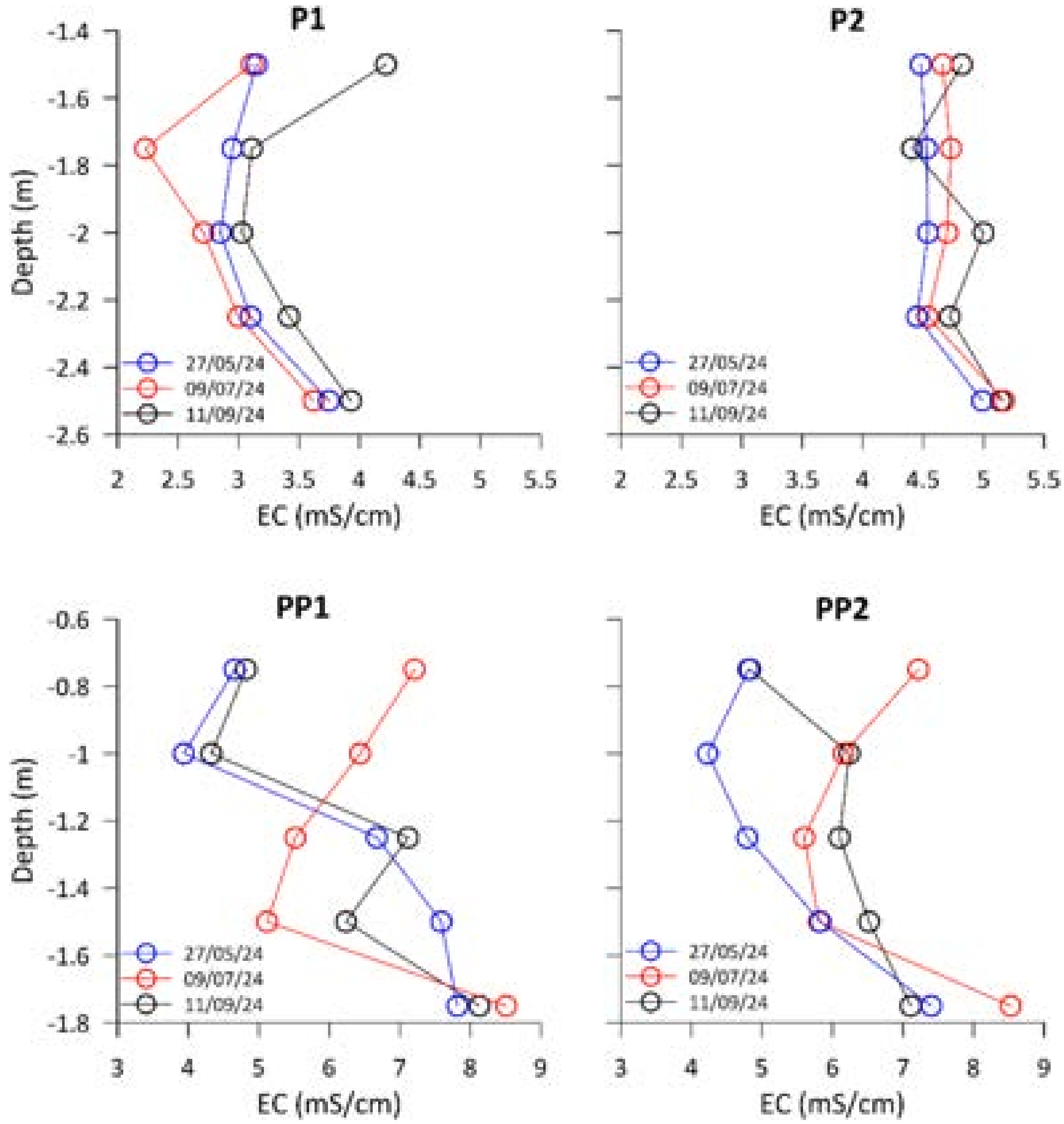

Fig. 7. Vertical profiles of EC in 3 sampling campaigns in the MLSs of P1 and P2 (A1 plot) and PP1 and PP2 (A2 plot).

Tab.2). The analysis on LF domain (avoiding daily fluctuation more related to atmospheric temperatures oscillation) revealed that the correlation between soil and GW temperature sharply increased considering only the sub-irrigation period instead of the whole monitoring period (see Supplementary Information) due to the rise of GW table promoting stronger capillary rise.

3.3. Cumulative salt export

Fig. 8 shows the outflow rate during the monitoring period, which was characterized by extremely low flow rates except for some peaks immediately after the heavy rainfalls of September-October 2024. During the sub-irrigation periods, the flow rate was often exceeding 5 l/s.

The salt export behaviour was clearly affected by the sub-irrigation periods when a steep increase was recorded. In fact, over the 84.5 ± 8.0 tons of salt exported during the monitoring period, approximately 67.2 ± 6.5 tons were exported during the sub-irrigation periods, which correspond to 80 % of the cumulative salt exported. Finally, although the salt export from A1 and A2 cannot be independently calculated, the contribution of A1 was much lower than A2, given that the EC in SW1-2 was lower than the EC in SW2 during the sub-irrigation periods (Fig. 6b).

Moreover, the EC monitored along the SW1 and SW2 ditches in September 2024 slowly increased from 0.55 to 2.0 mS/cm along the SW1 ditch draining A1, while abruptly increased up to 6.5 mS/cm in SW2 ditch draining A2 (see Tab. 1).

4. Discussion

This study has shown that an extreme spatial variability of GW salinity could be present in lowland reclaimed environments due to the uneven spatial distribution of peaty lenses. The latter can be considered as a long-term source of salinization, with salts entrapped within the peat fragments that can store and release large quantities of salts (Habakaramo Macumu et al., 2024). The presence of paleochannels can significantly lower the salinity, acting as a preferential pathway for solutes migration when they are located in topographic highs, as in this case, but they could also focus the upward GW flux and promote SW salinization if located in low-lying zones (de Louw et al., 2011). Thus, the topography is another salinity driver, since in low-lying zones the vadose zone is usually thinner (like in A2) and the saline GW is closer to the root zone, eventually provoking a higher crop' mortality or impairing crop yield. Capillary rise largely contributes to salts' upward transport, especially in A2, due to the concomitance of shallow GW table

Table 2
Correlation matrix of the larger significant (<-0.70 or >+0.70, p-values < 0.01) statistical parameters (P/K/S) for the LF component during the sub-irrigation periods.

	P2 GWL (A1)	PP1 GWL (A2)	VWC −30 cm (A2)	VWC −60 cm (A2)	PP1 T (A2)
VWC −35 cm (A1)	0.85/ 0.81/ 0.95				
VWC −45 cm (A1)	0.86/ 0.86/ 0.96				
PP0 GWL (A2)		0.94/ 0.72/ 0.86			
EC_{pw} −30 cm (A2)			0.93/0.78/ 0.94		
EC_{pw} −60 cm (A2)				−0.92/- 0.83/-0.96	
T_{soil} −30 cm (A2)					0.77/ *0.53/* 0.77
T_{soil} −60 cm (A2)					0.92/ 0.74/ 0.90

In *italic* are displayed smaller correlation coefficients (0.01 < p-values < 0.05).

and high salinity (van de Craats et al., 2020). Also the temperature monitoring in both vadose and saturated zone helped to support the interpretation of upward saline seepage from the aquifer to the vadose zone; in fact, the increase in correlation among soil T and GW T during the sub-irrigation period, confirms that heat is suitable as a tracer for GW fluxes direction intensity (Anderson, 2005; Kurylyk et al., 2019; Schmidt et al., 2024).

The fact that EC did not decrease in GW even in piezometers located near to the irrigation ditch and near to the tile drains, where GW levels followed SW levels' trend, is a clear indication that additional sources of salinity were present at the site, as recently pointed out by Habakaramo Macumu et al. (2024). The large and prolonged increase, with respect to the 0.5 mS/cm of the inlet, witnessed that the salt leaching was not driven by an advection mechanism (the so-called piston flow), but rather by dispersive and diffusive mechanisms from a dual-domain porous media (Zhang et al., 2024). The higher EC values of SW2 compared to SW1-2 values indicated a much larger contribution of A2 with respect to A1 in the salinization of SW resources.

This study has also shown that salt tolerant weeds are a source of salt that could be released in the unsaturated zone if not removed from the field, as pointed out by a recent study by Yin et al. (2023). Thus, besides the saline endmember of this system that is located in peaty lenses present both in the vadose zone and in the saturated zone, another source of salinity is related to the mulching of salt tolerant weeds. These salts can accumulate during the summer and slowly transported towards the saturated zone via recharge during wintertime in agricultural fields without tile drains, while could partially exported towards the surface water network in agricultural fields equipped with tile drains (Colombani et al., 2019).

Upwards seepage of saline GW is constant over the year in A2, as demonstrated by the frequency domain and correlation analyses, often reaching the tile drains where the salt may partially accumulate within and near the tiles. When the sub-irrigation is activated, the tile drains are backflushed, and the salt is exported quickly to the SW. This is proved by the fact that a remarkably high yearly salt export rate was calculated (19.7 ± 1.9 t/ha/y) and approximately 80 % of the cumulative salt was exported during the sub-irrigation periods, a value that is comparable to the one computed by Su et al. (2005) for similar environmental settings at the plot scale and even at the entire Polder basin during peak flow events (de Louw et al., 2011). But it is nearly 50 % higher than another typical Polder setting without subsurface irrigation (Delsman et al., 2014). It must be stressed that, although installed five years before, these drains were used for sub-irrigation purposes just from 2023; thus, the monitored period was the second sub-irrigation season, and the salt export could change in the next years. To prove this behaviour on the long term it is critical to continue monitoring this area for the coming years to understand if this mechanism will perform steadily or if the salt export will decrease or increase with time. A recent modelling study performed on the aquifer scale (and not at the field site like the present work) already proved that the salt export towards the SW network has experienced a constant increase in the last decade (Gaiolini et al., 2024), due to the combination of increased evapotranspiration due to the ongoing CC and excess of summer irrigation provided by farmers to maintain the crops yield. Although the model did not account for shallow presence of peaty lenses that could further exacerbate the soil and water resources salinization process. In particular, in view of the projected CC that will lead to the exacerbation of the above mentioned processes, it is suggested to avoid the mulching of salt tolerant weeds, which instead have to be removed by the field (both the aerial and roots parts of the plants) to maximize the soil desalination. Being tile drains a short cut between the saline GW and the SW, they are at risk of worsening SW quality, so sub-irrigation should not be employed in fields where the water table is close to the ground level and where peaty lenses are abundant. Finally, it is suggested to improve the monitoring in similar agricultural fields both in space and over a long period to confirm the finding of this paper and to proof whether saline GW upward

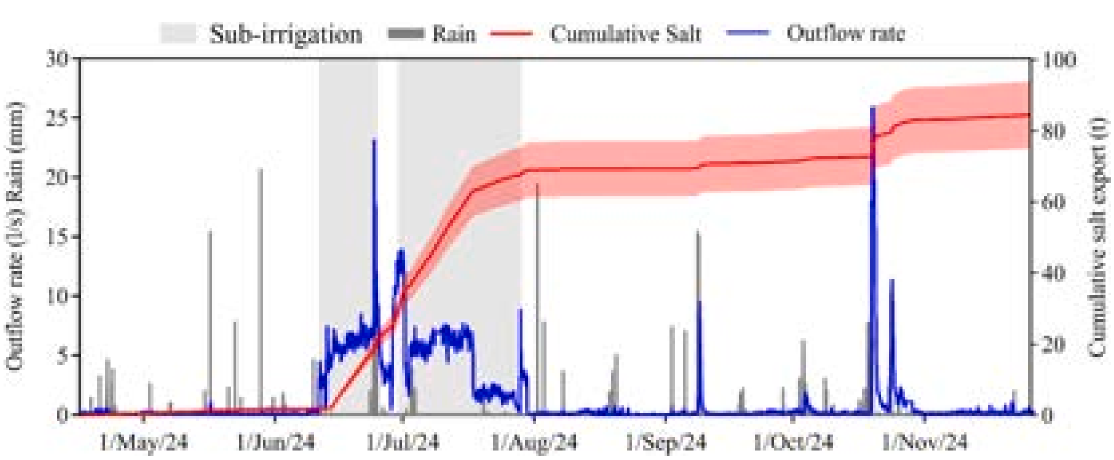

Fig. 8. Time-series plot of rainfall (mm), SW2 outflow rate (l/s), and cumulative salt export from A1 and A2 plots; sub-irrigation periods and the confidence intervals of the cumulated salt export (red shaded area) are also depicted. (For interpretation of the references to colour in this figure legend, the reader is referred to the web version of this article.)

induced by CC will possibly impair crop yield over large portions of this landscape.

5. Conclusions

This work presented a continuous monitoring approach, complemented with remotely sensed data to quantify exchange fluxes of water and dissolved salts in the vadose zone, GW, and SW out of a tile drained agricultural field characterized by saline soils. This salinization mechanism poses a serious threat to the SW resources that are used for irrigation in these reclaimed lands, especially considering the ongoing CC that has already put stress on the Po River lowland in the last years.

The employment of frequency domain analysis allowed to get more insights on these internal fluxes, like the upward saline flux during sub-irrigation periods in the vadose zone or the release of the large quantity of salts in porewater after the salt tolerant weeds mowing, that temporarily increased the porewater EC up to 20 mS/cm. This was due not only to the upward saline flux from GW, but also to the presence of halophilic vegetation fragments that slowly release salts into porewater and help to maintain elevated concentrations in GW and SW even after flushing many pore volumes.

The upward flux of saline GW also drives SW salinity with EC increase along the ditches draining the field up to 6.5 mS/cm. The water discharge and salt export were accurately quantified, and sub-irrigation resulted to boost salt flushing driving 67.2 tons of salt over the 84.5 tons exported during the whole monitoring period.

Despite the rigorous data processing and frequency domain analysis that helped in assessing GW saline fluxes and salt export through drainage ditches, many internal processes within the vadose zone remain uncertain (e.g., spatial variability of capillary rise and lateral flows) due to complex transpiration mechanisms that are difficult to quantify.

To maintain irrigation efficiency without the risk of salinization, differentiated strategies (e.g., surface irrigation when feasible, plant residual removal after mowing, controlled drainage from ditches) could help reducing salt release within the field.

Future works should be aimed at understanding the various sources of salinity that could play a role in the salinization of water resources in these reclaimed landscapes, with the aim to understand how to minimize such threats by implementing best management agricultural practices.

CRediT authorship contribution statement

Mattia Gaiolini: Writing – original draft, Software, Formal analysis, Visualization, Investigation, Data curation. **Chiara Sbarbati:** Validation, Investigation, Writing – review & editing, Supervision, Conceptualization. **Abraham Ofori:** Writing – review & editing, Data curation, Investigation. **Patrick Habakaramo Macumu:** Investigation, Formal analysis. **Maria Pia Gervasio:** Writing – review & editing, Investigation. **Elena Tamisari:** Resources, Writing – review & editing, Investigation. **Fabio Vincenzi:** Writing – review & editing, Data curation, Investigation. **Elisa Soana:** Validation, Writing – review & editing, Project administration. **Giuseppe Castaldelli:** Writing – review & editing, Resources, Validation. **Vincenzo Piscopo:** Writing – review & editing, Validation. **Micòl Mastrocicco:** Validation, Writing – review & editing, Supervision. **Nicolò Colombani:** Supervision, Investigation, Conceptualization, Writing – review & editing, Methodology, Data curation.

Declaration of competing interest

The authors declare that they have no known competing financial interests or personal relationships that could have appeared to influence the work reported in this paper.

Acknowledgements

We acknowledge the financial support under the National Recovery and Resilience Plan (NRRP), Mission 4, Component 2, Investment 1.1, Call for tender No. 104 published on 2.2.2022 by the Italian Ministry of University and Research (MUR), funded by the European Union – NextGenerationEU, Project Title NO3EXCESS – Nitrogen Origin, EXport and Cycling in coastal irrigatEd SettingS – CUP F53D23002160001 – Grant Assignment Decree No. 2022AKA3HL adopted on 30/06/2024 by the Italian Ministry of University and Research (MUR).

Appendix A. Supplementary data

Supplementary data to this article can be found online at https://doi.org/10.1016/j.jhydrol.2025.134563.

Data availability

Data will be made available on request.

References

Amorosi, A., Fontana, A., Antonioli, F., Primon, S., Bondesan, A., 2008. Post-LGM sedimentation and Holocene shoreline evolution in the NW Adriatic coastal area. GeoActa 7, 41–67.

Amorosi, A., Sammartino, I., 2007. Influence of sediment provenance on background values of potentially toxic metals from near-surface sediments of Po coastal plain (Italy). Int. J. Earth Sci. 96, 389–396. https://doi.org/10.1007/s00531-006-0104-8.

Anderson, M.P., 2005. Heat as a ground water tracer. Groundwater 43 (6), 951–968. https://doi.org/10.1111/j.1745-6584.2005.00052.x.

APHA (American Public Health Association), 2022. Standard Methods for the Examination of Water and Wastewaters, 24th ed.; APHA Press: Washington, DC, USA, 2022. ISBN: 978-0-87553-299-8.

Bellache, M., Torres-Pagan, N., Verdeguer, M., Llinares, J.V., Benfekih, L.A., Sestras, R.E., Vicente, O., Sestras, A.F., Boscaiu, M., 2022. Comparative analysis of tolerance to salt stress and water deficit in two invasive weeds of the Genus Erigeron (Asteraceae). Plants 11 (15), 2059. https://doi.org/10.3390/plants11152059.

Beltrán, J.M., 1999. Irrigation with saline water: benefits and environmental impact. Agric Water Manag 40 (2–3), 183–194. https://doi.org/10.1016/S0378-3774(98)00120-6.

Bonaldo, D., Bellafiore, D., Ferrarin, C., Ferretti, R., Ricchi, A., Sangelantoni, L., Vitelletti, M.L., 2023. The summer 2022 drought: a taste of future climate for the Po valley (Italy)? Reg. Environ. Chang. 23 (1), 1. https://doi.org/10.1007/s10113-022-02004-z.

Braca, G., Bussettini, M., Ducci, D., Lastoria, B., Mariani, S., 2019. Evaluation of national and regional groundwater resources under climate change scenarios using a GIS-based water budget procedure. Rend. Lincei-Sci. Fis. 30, 109–123. https://doi.org/10.1007/s12210-018-00757-6.

Bruno, L., Campo, B., Hajdas, I., Hong, W., Amorosi, A., 2022. Timing and mechanisms of sediment accumulation and pedogenesis: Insights from the Po Plain (northern Italy). Palaeogeogr. Palaeoclimatol. Palaeoecol. 591, 110881. https://doi.org/10.1016/j.palaeo.2022.110881.

Caschetto, M., Colombani, N., Mastrocicco, M., Petitta, M., Aravena, R., 2017. Nitrogen and sulphur cycling in the saline coastal aquifer of Ferrara, Italy. A multi-isotope approach. Appl. Geochem. 76, 88–98. https://doi.org/10.1016/j.apgeochem.2016.11.014.

Colombani, N., Mastrocicco, M., Castaldelli, G., Aravena, R., 2019. Contrasting biogeochemical processes revealed by stable isotopes of H_2O, N, C and S in shallow aquifers underlying agricultural lowlands. Sci. Total Environ. 691, 1282–1296. https://doi.org/10.1016/j.scitotenv.2019.07.238.

Da Lio, C., Tosi, L., 2019. Vulnerability to relative sea-level rise in the Po river delta (Italy). Estuar. Coast. Shelf Sci. 228, 106379. https://doi.org/10.1016/j.ecss.2019.106379.

de Louw, P.G.B., Eeman, S., Essink, G.O., Vermue, E., Post, V.E.A., 2013. Rainwater lens dynamics and mixing between infiltrating rainwater and upward saline groundwater seepage beneath a tile-drained agricultural field. J. Hydrol. 501, 133–145. https://doi.org/10.1016/j.jhydrol.2013.07.026.

de Louw, P.G.B., van der Velde, Y., van der Zee, S.E.A.T.M., 2011. Quantifying water and salt fluxes in a lowland polder catchment dominated by boil seepage: a probabilistic end-member mixing approach. Hydrol. Earth Syst. Sci. 15, 2101–2117. https://doi.org/10.5194/hess-15-2101-2011.

Delsman, J.R., Groen, M.M.A., Groen, J., Stuyfzand, P.J., 2014. Investigating summer flow paths in a Dutch agricultural field using high frequency direct measurements. J. Hydrol. 519, 3069–3085. https://doi.org/10.1016/j.jhydrol.2014.10.058.

Di Giuseppe, D., Faccini, B., Mastrocicco, M., Colombani, N., Coltorti, M., 2014. Reclamation influence and background geochemistry of neutral saline soils in the Po River Delta Plain (Northern Italy). Environ. Earth Sci. 72, 2457–2473. https://doi.org/10.1007/s12665-014-3154-4.

Duncan, R.A., Bethune, M.G., Thayalakumaran, T., Christen, E.W., McMahon, T.A., 2008. Management of salt mobilisation in the irrigated landscape–a review of selected irrigation regions. J. Hydrol. 351 (1–2), 238–252. https://doi.org/10.1016/j.jhydrol.2007.12.002.

Emery, W.J., Thomson, R.E., 2004. Data analysis methods in physical oceanography: third edition. Estuaries. https://doi.org/10.2307/1353059.

Erostate, M., Huneau, F., Garel, E., Ghiotti, S., Vystavna, Y., Garrido, M., Pasqualini, V., 2020. Groundwater dependent ecosystems in coastal Mediterranean regions: Characterization, challenges and management for their protection. Water Res. 172, 115461. https://doi.org/10.1016/j.watres.2019.115461.

Evett, S.R., Agam, N., Kustas, W.P., Colaizzi, P.D., Schwartz, R.C., 2012. Soil profile method for soil thermal diffusivity, conductivity and heat flux: comparison to soil heat flux plates. Adv. Water Resour. 50, 41–54. https://doi.org/10.1016/j.advwatres.2012.04.012.

Feist, S.E., Hoque, M.A., Ahmed, K.M., 2023. Coastal salinity and water management practices in the Bengal Delta: a critical analysis to inform salinisation risk management strategies in Asian Deltas. Earth Syst. Environ. 7 (1), 171–187. https://doi.org/10.1007/s41748-022-00335-9.

Gaiolini, M., Colombani, N., Chierici, V., Montanari, L., Mastrocicco, M., 2024. Numerical modelling of groundwater level and salinity evolution in a low-lying coastal area under intensive agricultural activity. Water Resour. Manag. 39 (4), 17747. https://doi.org/10.1007/s11269-024-04044-y.

Gao, B.C., 1996. NDWI—a normalized difference water index for remote sensing of vegetation liquid water from space. Remote Sens. Environ. 58 (3), 257–266. https://doi.org/10.1016/S0034-4257(96)00067-3.

Gervasio, M.P., Soana, E., Vincenzi, F., Magri, M., Castaldelli, G., 2023. Drought-induced salinity intrusion affects nitrogen removal in a deltaic ecosystem (Po River Delta, Northern Italy). Water 15 (13), 2405. https://doi.org/10.3390/w15132405.

Habakaramo Macumu, P., Gaiolini, M., Ofori, A., Mastrocicco, M., Colombani, N., 2024. Additional sources of salinity and heavy metals from plant residues of peaty horizons in the Po River lowland (Italy). Sci. Total Environ. 957, 177671. https://doi.org/10.1016/j.scitotenv.2024.177671.

Herrera-García, G., Ezquerro, P., Tomás, R., Béjar-Pizarro, M., López-Vinielles, J., Rossi, M., Mateos, R.M., Carreón-Freyre, D., Lambert, J., Teatini, P., Cabral-Cano, E., Erkens, G., Galloway, D., Hung, W.-C., Kakar, N., Sneed, M., Tosi, L., Wang, H., Ye, S., 2021. Mapping the global threat of land subsidence. Science 371 (6524), 34–36. https://doi.org/10.1126/science.abb859.

Hilhorst, M.A., 2000. A pore water conductivity sensor. Soil Sci. Soc. Am. J. 64 (6), 1922–1925. https://doi.org/10.2136/sssaj2000.6461922x.

Huete, A.R., 1988. A soil-adjusted vegetation index (SAVI). Remote Sens. Environ. 25 (3), 295–309. https://doi.org/10.1016/0034-4257(88)90106-X.

IBM Corp. Released 2024. IBM SPSS Statistics for Windows, Version 30.0.0.0 Armonk, NY: IBM Corp.

Jiao, J.J., Wang, Y., Cherry, J.A., Wang, X., Zhi, B., Du, H., Wen, D., 2010. Abnormally high ammonium of natural origin in a coastal aquifer-aquitard system in the Pearl River Delta, China. Environ. Sci. Technol. 44 (19), 7470–7475. https://doi.org/10.1021/es1021697.

Keegan-Treloar, R., Irvine, D.J., Werner, A.D., Banks, E.W., 2023. Identifying groundwater recharge and discharge zones using geostatistical simulation of hydraulic head and its derivatives. J. Hydrol. 617, 128993. https://doi.org/10.1016/j.jhydrol.2022.128993.

Kurylyk, B.L., Irvine, D.J., Bense, V.F., 2019. Theory, tools, and multidisciplinary applications for tracing groundwater fluxes from temperature profiles. WIREs Water 6, e1329.

Li, C., Gao, X., Li, S., Bundschuh, J., 2020. A review of the distribution, sources, genesis, and environmental concerns of salinity in groundwater. Environ. Sci. Pollut. Res. 27, 41157–41174. https://doi.org/10.1007/s11356-020-10354-6.

Lionello, P., Scarascia, L., 2018. The relation between climate change in the Mediterranean region and global warming. Reg. Environ. Chang. 18, 1481–1493. https://doi.org/10.1007/s10113-018-1290-1.

Loc, H.H., Lixian, M.L., Park, E., Dung, T.D., Shrestha, S., Yoon, Y.J., 2021. How the saline water intrusion has reshaped the agricultural landscape of the Vietnamese Mekong Delta, a review. Sci. Total Environ. 794, 148651. https://doi.org/10.1016/j.scitotenv.2021.14865.

Lu, N., Likos, W.J., 2004. Rate of capillary rise in soil. J. Geotech. Geoenviron. Eng. 130 (6), 646–650. https://doi.org/10.1061/(asce)1090-0241(2004)130:6(646).

Marchina, C., Bianchini, G., Natali, C., Pennisi, M., Colombani, N., Tassinari, R., Knoeller, K., 2015. The Po river water from the Alps to the Adriatic Sea (Italy): new insights from geochemical and isotopic (δ^{18}O-δD) data. Environ. Sci. Pollut. Res. 22, 5184–5203. https://doi.org/10.1007/s11356-014-3750-6.

Mastrocicco, M., Colombani, N., 2021. The issue of groundwater salinization in coastal areas of the mediterranean region: a review. Water 13 (1), 90. https://doi.org/10.3390/w13010090.

MathWorks Inc., 2023. MATLAB version: 9.13.0 (R2023b), Natick, Massachusetts: The MathWorks Inc. https://www.mathworks.com.

Montanari, A., Nguyen, H., Rubinetti, S., Ceola, S., Galelli, S., Rubino, A., Zanchettin, D., 2023. Why the 2022 Po River drought is the worst in the past two centuries. Sci. Adv. 9 (32), eadg8304. https://doi.org/10.1126/sciadv.adg8304.

Nicholls, R.J., Lincke, D., Hinkel, J., Brown, S., Vafeidis, A.T., Meyssignac, B., Hanson, S. E., Merkens, J.-L., Fang, J., 2021. A global analysis of subsidence, relative sea-level change and coastal flood exposure. Nat. Clim. Chang. 11 (4), 338–342. https://doi.org/10.1038/s41558-021-00993-z.

Petelet-Giraud, E., Cary, L., Cary, P., Bertrand, G., Giglio-Jacquemot, A., Hirata, R., Aquilina, L., Muniz Alves, L., Martins, V., Melo, A.M., Montenegro, S., Chatton, E., Franzen, M., Aurouet, A., the COQUEIRAL team, 2018. Multi-layered water resources, management, and uses under the impacts of global changes in a southern coastal metropolis: when will it be already too late? Crossed analysis in Recife, NE Brazil. Sci. Total Environ. 618, 645–657. https://doi.org/10.1016/j.scitotenv.2017.07.228.

Pugh, D. T., 1996. Tides, surges and mean sea-level (reprinted with corrections). John Wiley & Sons Ltd., ISBN 0 471 91505 X. http://eprints.soton.ac.uk/id/eprint/19157.

Seibert, S.L., Greskowiak, J., Oude Essink, G.H., Massmann, G., 2024. Understanding climate change and anthropogenic impacts on the salinization of low-lying coastal groundwater systems. Earth's Future 12 (8), e2024EF004737. https://doi.org/10.1029/2024EF004737.

Schmidt, C., Lewandowski, J., Galloway, J. N., Chalari, A., Ciocca, F., Krause, S., Pfister, L., Antonelli, M., 2024. Heat as a Hydrological Tracer. In Ecohydrological Interfaces (eds S. Krause, D. Hannah and N. Grimm). https://doi.org/10.1002/9781119489702.ch8.

Straffelini, E., Tarolli, P., 2023. Climate change-induced aridity is affecting agriculture in Northeast Italy. Agr. Syst. 208, 103647. https://doi.org/10.1016/j.agsy.2023.10364.

Su, N., Bethune, M., Mann, L., Heuperman, A., 2005. Simulating water and salt movement in tile-drained fields irrigated with saline water under a Serial Biological Concentration management scenario. Agric Water Manag 78 (3), 165–180. https://doi.org/10.1016/j.agwat.2005.02.003.

Tedeschi, A., Dell'Aquila, R., 2005. Effects of irrigation with saline waters, at different concentrations, on soil physical and chemical characteristics. Agric Water Manag 77 (1–3), 308–322. https://doi.org/10.1016/j.agwat.2004.09.036.

Thorslund, J., Bierkens, M.F., Oude Essink, G.H., Sutanudjaja, E.H., van Vliet, M.T., 2021. Common irrigation drivers of freshwater salinisation in river basins worldwide. Nat. Commun. 12 (1), 4232. https://doi.org/10.1038/s41467-021-24281-8.

Valipour, M., 2014. Drainage, waterlogging, and salinity. Arch. Agron. Soil Sci. 60 (12), 1625–1640. https://doi.org/10.1080/03650340.2014.905676.

van de Craats, D., van der Zee, S.E., Sui, C., van Asten, P.J., Cornelissen, P., Leijnse, A., 2020. Soil sodicity originating from marginal groundwater. Vadose Zone J. 19 (1), e20010. https://doi.org/10.1002/vzj2.20010.

van Vliet, M.T., Thorslund, J., Strokal, M., Hofstra, N., Flörke, M., Ehalt Macedo, H., Nkwasa, A., Tang, T., Kaushal, S.S., Kumar, R., van Griensven, A., Bouwman, L., Mosley, L.M., 2023. Global river water quality under climate change and hydroclimatic extremes. Nat. Rev. Earth Environ. 4 (10), 687–702. https://doi.org/10.1038/s43017-023-00472-3.

Viero, D.P., Roder, G., Matticchio, B., Defina, A., Tarolli, P., 2019. Floods, landscape modifications and population dynamics in anthropogenic coastal lowlands: the Polesine (northern Italy) case study. Sci. Total Environ. 651, 1435–1450. https://doi.org/10.1016/j.scitotenv.2018.09.121.

Wang, L., Iddio, E., Ewers, B., 2021. Introductory overview: Evapotranspiration (ET) models for controlled environment agriculture (CEA). Comput. Electron. Agric. 190, 106447. https://doi.org/10.1016/j.compag.2021.106447.

Yin, X., Feng, Q., Liu, W., Zhu, M., Zhang, J., Li, Y., Yang, L., Zhang, C., Cui, M., Zheng, X., Li, Y., 2023. Assessment and mechanism analysis of plant salt tolerance regulates soil moisture dynamics and controls root zone salinity and sodicity in seasonally irrigated agroecosystems. J. Hydrol. 617, 129138. https://doi.org/10.1016/j.jhydrol.2023.129138.

Zancanaro, E., Morari, F., Piccoli, I., Carrera, A., Zoccarato, C., Teatini, P., 2024. A novel technique to mitigate saltwater intrusion: freshwater recharge via drainpipe in permeable paleochannels. Hydrol. Process. 38, e15299. https://doi.org/10.1002/hyp.15299.

Zhang, J., Ye, Y., Lu, C., 2024. Salt leaching efficiency of subsurface drainage systems with mass transfer limitations. J. Hydrol. 632, 130940. https://doi.org/10.1016/j.jhydrol.2024.130940.